Soft Matter

Accepted Manuscript

ROYAL SOCIETY OF CHEMISTRY

www.rsc.org/softmatter

Fine structures of self-assembled beta-cyclodextrin/Pluronic in dilute and dense systems: a small angle x-ray scattering study

Kuo-Chih Shih[a], *Chi-Yen Li*[b], *Wen-Hsien Li*[b**] *and Hsi-Mei Lai*[a*]

[a] Department of Agricultural Chemistry, National Taiwan University,
No. 1, Roosevelt Rd., Sec. 4, Taipei 10617, Taiwan.
[b] Department of Physics, National Central University,
No. 300, Jhongda Rd., Jhongli, 32001, Taiwan.

***Correspondence to:**
Dr. Hsi-Mei Lai (E-mail: hmlai@ntu.edu.tw)
Telephone: +886-2-33664816
Fax: +886-2-23633123

****Co-Correspondence to:**
Dr. Wen-Hsien Li (E-mail: whli@phy.ncu.edu.tw)
Telephone: +886-3-4227151 ext 65335

Abstract

The evolution of the fine structures of self-assembled polypseudorotaxane (PPR) in Pluronic (PL F108) solutions containing dilute to dense beta-cyclodextrin (β-CD) was illustrated for the first time by small angle x-ray scattering (SAXS). Dense β-CD (~19 w/v%) was found feasible to be dispersed in 24% citric acid solution. Five percentage of PL F108 formed cylindrical micelles of 1 nm in radius and 8 nm in length in the presence of 24% citric acid through the dehydration of citric acid and citrate. PPR was formed through the host-guest interaction between PL F108 and β-CD. In dilute β-CD system (1%), the single chains of PPR with separated β-CD stacks on PL F108 were formed. The numbers of β-CD in each stack increased from 1 to 4 with increasing β-CD concentration to 9%. In dense β-CD system, PPR condensed to correlated structures majorly composed of two unit blocks through the hydrogen bonds between PPRs. Two distinguishable correlated domains with correlation lengths of 50 nm (marked α-phase) and 46 nm (marked β-phase) along the chains, but without fine periodic structure within each individual domain, were identified in the 10% β-CD solution. Periodic stacking of β-CD in the domains developed in the 12% solution. As β-CD concentration increased from 12 to 19%, the correlated heights of α and β phases shrank from 41 and 32 nm into 30 and 10 nm, respectively. There were 48 β-CDs that stabilized on each PL F108 chain in the 19% β-CD system, which is in a good agreement with the stoichiometry.

Keywords: self-assembly, polypseudorotaxane, Pluronic, β-CD, SAXS,

Introduction

Cyclodextrins (CDs) are alpha-1,4 linked cyclic oligosaccharides, mainly consisting of 6, 7 or 8 alpha-D-glucopyranose units, known as alpha-, beta- or gamma-CD, respectively.[1] The hydrophilicity of the outer rims and the relative hydrophobicity inside cavities render CDs to form stable inclusion complexes (ICs) with organic molecules, such as flavours, pigments, vitamins and drugs.[2, 3] In addition, the formation of sequential ICs of several CD molecules within one polymer chain leads to a unique supramolecule, namely the polypseudorotaxane (PPR).[4] The driving forces of this self-assembling process include the hydrophobic interaction between polymers and CD cavities, the hydrogen-bonding among the rims of neighbouring CD on the same polymer chain, and the subsequent loss of PPR solubility.[5]

Pluronic® (PL) is a triblock copolymer with a configuration of PEG-PPG-PEG. It is a nonionic surfactant and has been widely used in pharmaceutics on taking the advantage of its self-assembling ability.[6] At its critical micelle concentration (CMC), the hydrophobic interaction among PPG segments and the phase separation between PEG and PPG blocks attributed to their various hydrophobicity in the solution induce the micellization.[1] However, the self-assembled structure of PL in solution can vary not only with its concentration,[7] but also be affected by the presence of organic or inorganic salt, such as potassium chloride,[8, 9] sodium chloride,[10-12] sodium carbonate,[13] and salicylic acid.[14]

When introducing CDs into PL, several CDs can thread onto the PPG or PEG segments of the PL to form PPRs. The interaction between CDs and PL blocks has been studied, through which various nano-structures have been identified in the solutions containing CD and PL. These include dissolute[15-17] or growing micelle,[18]

hollow sphere,[19] rod-like[16] and platelet structures[18, 20] that have all been characterized by using small angle x-ray/neutron scattering (SAXS/SANS).

Restricted by the low solubility of native β-CD (1.85 g/100 mL water at 25°C), modified β-CD was commonly used in investigating the self-assembled structures of PPR. Previous studies of β-CD based PPR were focused either on low concentration of native β-CD or on high concentration of modified β-CD.[16, 21] It has been realized that the solubility of β-CD can be effectively enhanced by using organic acids, such as citric acid, lactic acid and malic acid.[22, 23] Studies made on the nanostructures of PPRs at high native β-CD concentrations are then possible in an aqueous system containing organic acids. In fact, β-CD can be evenly dispersed in citric acid solution, with a solubility that is 10 times higher than in pure water.[24] The role of citric acid is to break the hydrogen bonds among β-CD molecules.[25]

In this study, the evolution of nanostructure of β-CD/PL in citric acid solution containing 5% PL F108 and various β-CD concentrations (0~19%) were investigated by SAXS measurements. SAXS measurement is capable in identify the correlated structure in the nanometer scale and is suitable for examining the self-assembling structure of PL F108 itself and β-CD/PL systems. Analysing the SAXS patterns with appropriate models allow quantitative extractions of PL F108 and β-CD based PPR structures in citric acid solution, which provide detailed insights of these self-assembled supramolecules.

Experimental section

Materials

PL F108 (EG_{133}-PG_{49}-EG_{133}, Mw 14600 g/mol) was purchased from BASF (Florham Park, New York, USA). β-CD (purity ≥ 97%) was obtained from Sigma-Aldrich (St. Louis, MO, USA). All chemicals used in the present study were analytical grade.

Preparation of PL F108 and β-CD/PL samples

A β-CD stock solution (20 w/v% β-CD) was prepared with 24% citric acid solution. Before mixing with the β-CD stock solution, an adequate amount of PL F108 pellet was dissolved with 24% citric acid solution as well. Results of our measurements show that the 24% citric acid solution can effectively separate β-CD molecules, resulting in a clear and well dispersed solution. Below which, the aggregations of β-CD are able to be detected by vision. The depletion of flocculation due to the decrease of dispersibility had been reported when a high concentration of citric acid is used.[26, 27] In order to minimize the scattering background contributed by citric acids, the 24% citric acid solution was chosen as the solvent in this study. The β-CD/PL mixtures contained various concentrations of β-CD (0-19%) and 5% PL F108 in 24% citric acid solutions. The mixtures were stored at 6 ± 2°C for 12 h and then at 25°C for an additional 24 h before taking SAXS measurements. This process amounts to a total setting time of 36 h for the β-CD/PL in the solution. The concentrations of PL F108 and β-CD were used to mark the samples. As an example, 5-19 indicates the sample contains 19 w/v% β-CD and 5 w/v% PL F108 in the 24% citric acid solution.

Small angle X-ray scattering (SAXS) measurement

The SAXS experiment was performed on the beamline 23A1, operated in the transmission mode, at National Synchrotron Radiation Research Center (NSRRC), Taiwan. The sample was loaded in a standard solution cell for the measurement, sealed with kapton films. The data were collected using photons of incident energy 12

keV (incident wavelength λ = 1.033 Å), with a sample-to-detector distance of ~3 meters. This setup provides a q-range from 0.006 to 0.28 $Å^{-1}$ available for measurements, where scattering vector $q = 4\pi\sin\theta / \lambda$ and θ is half of the scattering angle.

SAXS data analysis

It has been known that the radius of gyration (R_g) of the scattering object in solution can be obtained from Guinier analysis,[28] and the pair distance distribution function (PDDF) can be extracted from the indirect Fourier transform (IFT) analysis[29] of the scattering profile. The PDDF was obtained by employing the GNOM program in the ATSAS suite, which was developed by the BIO-SAXS group at EMBL-Hamburg.[30] The model fitting method suggested by Yeh et al.[31] was used to separate the form factor P(q) from the structure factor S(q) that could appear in the scattering pattern I(q) = P(q)S(q). The form factor contains the intensity scattered from the shape of the object; whereas the structure factor links to the diffraction intensities from the periodic structure of the correlated domains. Two scattering profiles that link to form factor were considered: one models the low q (< ~0.01 $Å^{-1}$) scattering, while the other describes the high q scattering. The form factor was analyzed employing the IGOR Pro 6.11 program package provided by NIST (National Institute of Standard and Technology) Center for Neutron Research (NIST, Gaithersburg, MD, USA).[32] The structure factor, on the other hand, was analyzed by fitting the diffraction peaks to the diffraction profiles of finite-sized domains. It is known that the width of a diffraction peak reflect the spatial extension of the periodicity, which corresponds to the size of the correlated domain in the present cases. The line profile of a diffraction peak from a size-dispersed supramolecule assembly was obtained by combining the diffraction profiles contributed from each individual domain in the assembly. The line profile of

the structure factor was used to extract size distribution of the supramolecules in the solution. Details of the fitting processes will be described in the following sections.

Results and discussion

Qualitative analysis

SAXS measurements were carried out on the mixtures containing various concentrations of β-CD (0~19%) in 5% PL F108 that was prepared with 24% citric $acid_{(aq)}$. The scattering patterns were used to extract the micelle conformation and size as well as the stacking of polypseudorotaxane formed by ICs of β-CD and PL F108. The scattering patterns in Fig. 1 show clearly that the structures of PL F108 and β-CD changed significantly with the β-CD concentration. Interestingly, the scattering patterns can be divided into two groups according to their profiles. The samples, such as 5-0, 5-1 and 5-9, generate only scattering from the form factor are designated as the dilute systems; whereas those, such as 5-10, 5-12, 5-14, 5-16 and 5-19, producing diffraction peaks as well are designated as the dense systems.

The scattering patterns in the low-q regime (0.006 to 0.01 $Å^{-1}$) of the dilute systems can be expressed by the power law $I(q) = Aq^{-\alpha}$, with an exponent α around 2.5 (Fig. 1, 5-0, 5-1 and 5-9), signalling the existence of a large-scale structure in the dilute solutions. It is known that the mass and surface fractals will give rise to values of 1~3 and 3~4, respectively, for the scattering exponent. The low-q scattering with α~2.5 observed in the dilute systems reflects the scattering contributed mainly from the structure of the mass fractal. We believe that this large-scale structure is contributed from the PL F108 in the sample 5-0, and from the PL F108 as well as from the PPR in the samples 5-1 and 5-9. On the other hand, the scattering exponent in the high-q regime of the dilute systems was found to be near 1, reflecting the

scattering from elongated cylindrical objects. It is interesting to note that the onset of high-q scattering regime shifts from at $q \sim 0.07$ Å^{-1} for the sample 5-0 to $q \sim 0.16$ Å^{-1} for the sample 5-9, indicating the size of the cylindrical objects was reduced upon incorporating β-CD into the mixtures.

The appearances of diffraction peaks in the scattering patterns of the dense β-CD systems show that the interactions among the β-CDs have become strong enough to form correlated structures. As an example, the broad peak at $q = 0.013$ Å^{-1} in the 5-10 pattern (Fig. 1, 5-10) corresponds to a correlated size of 50 nm for the β-CD. The diffraction peaks shift gradually to larger q positions in the denser systems, indicating the correlated domains condensed into smaller sizes. Higher order diffraction peaks are clearly revealed in the samples with a β-CD concentration higher than 12%. In addition, a q^{-2} scattering profile was observed in the low-q regime of the dense systems, revealing scattering from two-dimensional (2D) geometry of lamellar. Interestingly, similar high-q scattering profiles were observed for the samples with β-CD concentration higher than 9%, showing the conformation of the small entities in the system has stabilized.

Guinier analysis of the dilute systems

Guinier region can be identified in the scattering profiles of samples 5-0, 5-1 and 5-9, expressed as $\mathrm{I}(q) \propto \exp(^{-R_g{}^2 q^2}/_3)$, where R_g is the gyration radius of the scattering object.[28] The absolute value of the slope in the $\mathrm{Ln}\{I(q)\}$ versus q^2 plot (Guinier plot) gives the value of $R_g^2/3$. The R_g values are 25.3, 7.14, and 7.75 nm for samples 5-0, 5-1 and 5-9, respectively. It is interesting to point out that a significant reduction (by a factor of ~3) in the aggregated sizes of PL F108 to PPR. Unfortunately, Guinier analysis is not possible to perform on the dense systems, where the low-q scattering

profile is severely disturbed by the appearance of diffraction peaks.

Indirect Fourier Transform (IFT) analysis

The IFT analysis is a model independent method to obtain information on the spatial distribution of mass density in the solution. This analysis gives the pair distance distribution function, $p(r)$ known as.

$$p(r) = \frac{1}{2\pi^2}\int_0^\infty I(q)qr\sin(qr)\,dq \quad (1)$$

where q is the magnitude of the scattering vector. This $p(r)$ gives the probability to find out a mass point at a distance r away from a selective point within the scattering object, weighed by the difference in scattering length density (SLD) between these two points. In the case of a rod-like object, the PDDF can be determined by $p(r) = \gamma_c(r) \times r$, where $\gamma_c(r)$ is the characteristic function of the thickness. Fig. 2 shows the $p(r)$ obtained for the dilute samples. All of three $p(r)$ distributions show a symmetric, Gaussian-like peak with a maximum at r = 0.5, 0.45, and 0.38 nm for the samples 5-0, 5-1, and 5-9, respectively. The shape of $p(r)$ displays a fixed SLD for the rod-like cylinder object over the entire cross-section.[29, 33, 34] It is known that PL formed core-shell micelle with a hydrophobic PPG core and a hydrophilic corona.[35] For sample 5-0 the cross-section of the rod-like micelle is composed of a PPG core with a SLD of ρ_{PPG} = 9.47 × 10^{-6} Å^{-2} and a PEG corona with a SLD of ρ_{PEG} = 1.11 × 10^{-5}Å^{-2}.[35] Only a cylindrical object could be identified with the weak scattering contrast between PPG core and PEG corona. For samples 5-1 and 5-9 the PPR is composed of a β-CD shell ($\rho_{\beta\text{-}CD}$ = 1.3 × 10^{-5} Å^{-2}) and a PL F108 core ($\rho_{PL\,F108}$ = 1.07 × 10^{-5} Å^{-2}). The scattering contrast between β-CD and 24% citric acid solvent (ρ_{sol} = 1.03 × 10^{-5} Å^{-2}) is much better than that between PL F108 and the solvent. We believe that the scattering profiles of samples 5-1 and 5-9 were contributed by the rod-like PPRs composed of numerous β-CDs. These results suggest that cylindrical objects,

but not core-shell cylinder ones, should be incorporated in describing the scattering profile.

Model fitting

Dilute systems (0, 1 and 9% β-CD)

As mentioned above, the scattering patterns of dilute systems can be modeled by a low-q power law and a high-q cylindrical conformation scattering. Hence, the expression for scattering profile should contains scattering from large-scale network[36] that can be formulated using the Debye-Anderson-Brumberger (DAB) model[37] and from the non-interacting cylinders in the solutions. Fig. 3 shows the observed (open squares) and calculated (solid line) scattering profiles of sample 5-0. The contributions from the cylinders (dashed line) and from the DAB model (dotted line) are displayed in Fig. 3 as well. The DAB model may be expressed as

$$I(q) = \frac{A\xi^2}{\left[1+\left(q\xi^2\right)\right]^2}, \qquad (2)$$

where ξ is the characteristic length of the domain size and A is a scale factor. The form factor of cylinder can be expressed as

$$P_{cyl}(q) = A\frac{1}{\pi r^2 L}\int_0^{\pi/2} f^2(q,\alpha)\sin(\alpha)d\alpha, \qquad (3)$$

where $f(q,\alpha) = 2(\rho_{cyl}-\rho_{sol})\pi r^2 L j_0(qL/2\cos\alpha)\frac{j_1(qr\sin\alpha)}{qr\sin\alpha}$, $j_0(x) = \sin(x)/x$, j_1(x) is the first order Bassel function, α is the angle between the axis of the cylinder and the scattering vector q, r and L are the radius and the length of cylinder, respectively. $\rho_{cyl} = 1.07 \times 10^{-5}$ Å^{-2} and $\rho_{sol} = 1.03 \times 10^{-5}$ Å^{-2} are the SLD of PL F108 and 24% citric acid solution, respectively. The fit allows extracting r and L of the cylinder.

Dense systems (10, 12, 14, 16 and 19% β-CD)

The structure factor $S(q)$ could be extracted by separating the form factor $P(q)$ from the scattering pattern $I(q)$. Taking the pattern of sample 5-19 (Fig. 4) as an example, the form factor contributed from the lamellar structure was expressed as

$$P_{lam}(q) = \frac{2\Delta\rho^2}{q^2}\left[1-\cos(q\delta)e^{-q^2\sigma^2/2}\right], \quad (4)$$

where Δρ is the scattering contrast between the lamellar structure (β-CD) and the solvent (24% citric acid solution), σ is the mean variation of the layer thickness, δ is the thickness of lamellar structure. On the other hand, the scattering contributed from the cylinder structure (revealed more clearly in the high-q regime) of the dense systems is complicated by the diffraction peaks (Fig. 1). The form factor associated with the cylinders of sample 5-9 was then adopted for that of dense systems. This is justified since the scattering from the cylinders has stabilized in systems with a β-CD concentration higher than 9%, as can be seen in Fig. 1. The scattering contributed from form factor was thus expressed as the linear combination of $P_{lam}(q)$ and $P_{cyl}(q)$ with a cut-off wave vector[38] q_0 in weighting the two contributions,

$$P(q) = \mathrm{A}\exp\left(-\frac{q}{q_0}\right)^{5.33} \times P_{lam}(q) + \mathrm{B}\exp\left[1-\exp\left(-\frac{q}{q_0}\right)^{5.33}\right] \times P_{cyl}(q), \quad (5)$$

where A and B are the intensity scale factors. In this form the lamellar form factor dominates in the low-q ($q < q_0$) regime, while the cylinder form factor dominates in high-q's.

Structure factor is expressed using the Debye-Scherrer equation with Gaussian peak profiles as

$$I_{hkl}(\theta) = \frac{1}{(w/2)\sqrt{2\pi}}\exp\left[\frac{-(\theta-\theta_c)^2}{2(w/2)^2}\right], \quad (6)$$

where θ is the half of the scattering angle, θ_c is the peak position, and w is the full width at half maximum of the peak profile. The pattern of sample 5-19 was thus separated into three contributions of from the cylinders in the mixture (open triangles, marked $P_{cyl}(q)$ in Fig. 4), from the lamellar conformation (open circles, marked $P_{lam}(q)$ in Fig. 4), and from periodically correlated β-CD (dotted lines in Fig. 4).

Effect of β-CD concentration on PPR structure

Nanostructure of β-CD/PL F108 in dilute systems

In this section, we focus on analyzing the structure of the cylinders in the mixture. Fig. 5 shows the observed and calculated patterns of samples 5-0, 5-1 and 5-9, where no diffraction peaks are revealed yet. A rod-like cylinder with $r \sim 1$ nm and $L \sim 8$ nm were obtained in the sample 5-0. It is known that R_g of an elongated object has been calculated to be $(\frac{r^2}{2} + \frac{L^2}{12})^{\frac{1}{2}}$ and it was calculated to be 24.7 nm for 5-0 sample. This is in good agreement with the R_g value (25.3 nm) extracted from the Guinier analysis. This cylindrical object is understood to be the micelle formed from PL F108 originated from the hydrophobic interaction between the PPO segments in the mixture. Cylindrical micelle has been observed in PL F108 in 0.5 M sodium carbonate aqueous solution.[13] Cylindrical micelle of other PL series has also been observed in inorganic salt[8-12] and in butan-1-ol.[39] In the present systems, citric acid dissociates 1 proton in 24% citric acid solution with a pH value of 1.5. We believed that the citric acid and its conjugated salt, known as citrate, are responsible for the dehydration process to form cylindrical PL F108 micelles. Similar phenomenon has also been observed in a separated study.[14]

It is known that characteristic length ξ can be used to describe the large-scale network structure in the mixture of PL F108 and citric acid using the DAB model.[36] A

characteristic length of 28.3 nm for the network in sample 5-0 is identified. This network is formed from the entanglement of the unassociated PL F108 unimer in the mixture. The citric acid is believed to play a crucial role in the formation of the extended network, initiated by the development of hydrogen bonds between citric acid and PL F108.

Introducing β-CD into PL F108 drives the onset of q^{-1} behavior in the scattering pattern to appear at larger q (Fig. 5, 5-0 and 5-1), indicating the formation of smaller cylindrical objects. These objects are the rod-like PPR[38] formed through the host-guest interaction between β-CD and PL F108. In sample 5-1, the molar ratio between PG and β-CD is 19.6, the PL micelle will not be fully de-assembled. We believe that both PL F108 micelle and rod-like PPR co-exists in the mixture, since the scattering from micelle vanished once PG/β-CD was below 3.1.[16] However, only the scattering from rod-like PPR were identified in the scattering pattern of sample 5-1. As mentioned above the scattering contrast between 24% citric acid solution (1.03×10^{-5} Å^{-2}) and β-CD (1.3×10^{-5} Å^{-2}) is known to be considerably better than that of between 24% citric acid solution and PL F108 ($\sim 1.07 \times 10^{-5}$ Å^{-2}).[40] It is clear that the scattering pattern in the $q > 0.1$ Å^{-1} regime is dominated by the scattering from β-CD, and reflects the morphology of the stacking of β-CD on PL F108.[41] Table 1 lists the fitted parameters for the samples 5-0, 5-1 and 5-9. The correlated β-CD block was found to be of 0.6 nm in radius and 1.2 nm in length, revealing that single chains of PPR with a stacking of 1 or 2 correlated β-CDs in each unit block were formed in these samples. We note that the radius and length of one β-CD are known[1] to be 0.77 and 0.79 nm, respectively.

The scattering patterns in the $q < 0.1$ Å^{-1} regime of samples 5-1 and 5-9 are nearly identical (Fig. 4). The differences in the two patterns are, however, seen at $q > 0.1$ Å^{-1}

reflect the structure of the rod-like PPRs are indeed different. The length of PPR increased from 1.2 nm for sample 5-1 to 2.4 nm for sample 5-9 (Table 1), showing the number of stacked β-CD has increased to 3 or 4 β-CD in each correlated block. In the mixture containing α-CD and PEO homopolymer in H_2O, the rod-like PPR self-assembled with 7 CDs per stacking block.[41] The number of CD stacked in each block on PL F108 depends on the strength of inter-CD hydrogen bonding (head-to-head or tail-to-tail).[41, 42] It is known that β-CDs can be dispersed in citric acid solution through the hydrogen bonds among the polar groups (-COOH and -OH) of citric acid and the -OH groups of β-CD located on its outside rim.[25] Therefore, the interaction of inter-CD hydrogen bonds in citric acid solution is less effective than those in H_2O. This results in a less number of CDs that are stacked in the present mixtures. In sample 5-9 of molar ratio PG/β-CD = 2, a PPG segment[43] that is fully covered by β-CD can be expected. Thus, a rod-like PPR with a length of ~20 nm can be expected in sample 5-9. Interestingly, only cylinders with a length of 2.4 nm were observed in sample 5-9. This suggests that there are numerous separated short PPR instead of forming fewer long rod-like PPRs in 24 w/v% citric acid solution. We hence propose that the β-CDs not only thread onto the PPG segments but also on the PEG segments in considerable portions. The formation of β-CD inclusion complex with PPG homopolymer in the presence of citrate ions has been observed in a previous study.[44] β-CD has been found to form inclusion complex, with noticeable amount of β-CDs, being reside on PEG segments of PL P85.[45] It has been reported that the binding constant of naproxen with β-CD in the presence of 1% PEG would be reduced that was attributed to the formation of PEG-β-CD inclusion complexes; therefore, the amount of free CD available for the inclusion with naproxen was reduced.[46]

Through DAB model calculations, the domain size in each sample was identified. These results are summarized in Table 1. A domain size of 28.3 nm was obtained for PL F108 (sample 5-0). The domain size decreases to 18.5 nm in sample 5-1, and further to 15.5 nm in sample 5-9. The driving force for a shorter characteristic length in higher β-CD concentration is believed to be due to the stronger inter-CD interaction in higher β-CD environment in the PPR chains and among the rims of the neighboring CD.[5] In our previous work[24], similar results were observed in the sample containing a higher molar ratio of PG/β-CD = 17.6, where PPR gels formed with the assistance of cross-link PPR crystallines resulting from the attractive interaction in neighboring PPRs.

Nano structure of β-CD/PL F108 in dense systems

Fig. 6 shows the observed and calculated scattering patterns of the dense samples. Through this analysis, the structure factor is effectively extracted from the scattering intensity for further analysis. The diffraction peaks were mainly contributed from the periodic structure of β-CD, since the scattering contrast of β-CD is significantly higher than that of PL F108. The isolated diffraction pattern of sample 5-10 is shown in Fig. 7, where two diffraction peaks can be identified. The intense one corresponds to a domain size of 50 nm ($d = 2\pi/q$), marked as α-phase with $c_\alpha = 50$ nm; whereas the less intense one corresponds to a domain size of 96 nm, marked as β-phase with $c_\beta = 96$ nm. It is known that the width of a diffraction peak reflect the spatial extension of the lattice periodicity, which could be used to extract the stacking height of the correlated β-CD. The line profile of a diffraction peak from a size-dispersed assembly can be obtained by combining the diffraction profiles contributed from each correlated grain in the assembly. The solid curves in Fig. 7 indicates the calculated diffraction profile with the size distributions of the two phases shown in the inset to

Fig. 7, assuming the sizes consist of multiple stacking of the c_α or c_β unit blocks. It is interesting to find that most of the correlated β-CDs in both phases interconnected into stacking of two unit blocks of stacking heights d_α = 96 nm and d_β = 188 nm. Moreover, the intensity of the α-phase is considerably higher (3.2 times more intense), showing that most of the correlated β-CDs condensed in the α-phase. There is no higher order reflections that appear in the diffraction pattern, showing the condensed β-CDs within the unit blocks are not packed into periodic structure yet.

Two sets of the diffraction peaks with different intensity could be identified in the samples 5-12 and 5-14. The more intense one, that is the α-phase, shrinks to a shorter spatial period of c_α = 41 nm, while the β-phase shrinks to c_β = 32 nm (Fig. 8). This is understandable that the correlated β-CDs will condense into a more compact structure in a solution with higher β-CD concentration. The peak widths of the β-phase are much broader than those of the α-phase, indicating that α and β phases are originated from separated structures. In addition, the size analysis based on the diffraction profiles giving 94% of the α-phase and 95% of the β-phase are composed of two unit blocks in sample 5-14, as shown in the inset in Fig. 8. Higher order diffraction peaks of up to the (003) reflection associated with both phases are revealed in the diffraction pattern, indicating the β-CDs in the unit blocks have built up periodic structures to form shorter periodicities. It is known that the total diffraction intensity is directly proportional to the mass of the phase that generates the diffraction pattern. The intensity ratio between that from the α-phase and from the β-phase can be used to calculate the mass ratio of the two phases in the solution. A mass ratio of m_α/m_β = 73/27 was obtained for sample 5-14, when taking the diffraction intensity is dominated by the mass of the unit block. This can be justified since the main difference between the α-phase and β-phase is the numbers of β-CD that are

correlated into the unit block. The α-phase shrinks into a periodicity of c_α = 30 nm in samples 5-16 and 5-19. Higher order diffraction peaks of up to the (008) reflection are revealed, but no sign of the existence of the (009) reflection in the measured diffraction pattern, as shown in Fig. 9. This suggested that a long-range ordering structure composed of β-CD was formed. The appearance of (008) reflection in the diffraction pattern indicates that there are at least 16 correlated β-CDs condensed in each 30 nm unit block, which corresponds to a separation of (30/16)-0.8=1.075 nm between the neighboring β-CDs in the correlated structure. The other possible structure is that there are 24 correlated β-CDs in each 30 nm unit block, which then gives a separation of (30/24)-0.8=0.45 nm between the β-CDs. The α-phase in sample 5-19 composes of two unit blocks, that is, at least 32 (16×2) and 48 (24×2) β-CDs could be identified on one polymer chain, respectively. In addition, the molar ratio of PG/β-CD = 1 for sample 5-19 which represented at least 49 β-CDs on a polymer chain, assuming β-CD distributed equally in each polymer chain. We, hence, conclude that the short separation of 0.45 nm between the β-CDs is likely to occur in sample 5-19.

A schematic representation of the evolution of the ordered structure of β-CDs in PPR with β-CD concentration is illustrated in Scheme 1. In sample 5-10, the β-CDs loosely aggregate into alternative stacking of a dense segment of 50 nm in length and a dilute segment of 46 nm long (Scheme 1 (a)). The mass density of the dilute segment is ~31% that of the dense one. On the average, the β-CD coated PPR chains bend in every two alternative stacking. This structure generates two diffraction peaks at periodicities of 50 and 50+46=96 nm, but no higher order peaks. In samples 5-12 and 5-14, the interaction among β-CDs is apparently strong enough for the aggregated β-CDs not only condense into a shorter separation, but also correlate into a periodic structure. The dense segment condenses into a spatial extension of 40 nm, while the

dilute one shrinks to 32 nm long (Scheme 2(b)). It is the two correlated structures that generate the two series of diffraction peaks. In the denser mixtures of samples 5-16 and 5-19, there are 24 correlated β-CDs that packed into a unit segment of 30 nm long, but no significant amount of correlated β-CD that appears in between the unit segment (Scheme 1 (c)).

As mentioned above, the scattering pattern of sample 5-9 can incorporated directly in the fitting process to model the high *q* scattering for samples in the dense β-CD system. Two possibilities can contribute to this result. First, these rod-like PPRs are the building blocks of the lamellae. Second, these rod-like PPRs does not condensed into the lamellar structure but remain in the 'freely dispersed' form in the solution. Based on the fact that the periodic structure composed of 24 β-CDs, the later scheme is likely to occur in the present systems.

Schematic representation of β-CD/PL F108 in citric acid solution

A schematic representation of the nano-structure in the mixtures with or without β-CD is shown in scheme 1. PL F108 forms cylindrical micelle in 24 w/v% citric acid solution [Scheme 2(a)]. With the addition of 1% β-CD, a rod-like PPR is formed with 1~2 CDs that are aggregated in each threaded β-CD stack [Scheme 2(b)]. For the system with 9% β-CD in the mixture, the number of CD in the β-CD block increases to 3~4 units, and the characteristic length decreases, which we believe is triggered by the formation of hydrogen bonds between β-CDs [Scheme 2(c)]. In addition, β-CD can thread not only on the PPG segment but also on the PEG segment of the PL F108 chain. Increasing β-CD concentration further to 19%, the aggregated structure

develops into a periodic arrangement, with 24 β-CDs condensed into a unit block [Scheme 2(d)]. Moreover, small but noticeable amount of PPR single chains remain in the 'freely dispersed' form surrounding the ordered structure.

Conclusion

Investigated by small angle x-ray scattering measurements, the self-assembled structures of PL F108 in 24% citric acid solution containing 0 to 19% β-CD were revealed. PL F108 forms cylindrical micelles in 24% citric acid solution, originated from the dehydration effect of citric acid and citrate. The threaded β-CDs formed numerous separated short PPR not only on the PPG segment but on the PEG segment instead of long single chain PPR in the dilute systems. The attractive interactions among neighboring β-CDs on the single PL F108 chain and among the PPR single chains, presumably through the hydrogen bonding, result in shorter characteristic length. In the dense systems, the attractive interactions drive the β-CDs to pack into a periodic structure. The size of the periodic structure decreased with increasing β-CD concentration in the mixture. Furthermore, the number of the β-CDs on single PL F108 chain has also been revealed.

Acknowledgements

This work was supported by the Grants NSC 98-2313-B-002-050-MY3 and 102-2313-B-002-056-MY3 from the National Science Council, Taipei, Taiwan. We thank Dr. Ya-Sen Sun of the Department of Chemical and Materials Engineering, National Central University, Taiwan and Dr. U-Ser Jeng of the NSRRC for discussion.

References

1. J. Szejtli, in *Chemical and functional properties of food saccharides*, ed. P. Tomasik, CRC Press, Boca Raton, 2004, ch. 17, pp. 259-277.
2. H. Hashimoto, *in Comprehensive supramolecular chemistry,* ed. J. M. Lehn, Pergamon, Oxford, 1996, vol. 3, ch. 16, pp 483-502.
3. L. S. Szente, J., in *Comprehensive supramolecular chemistry*, ed. J. M. Lehn, Pergamon, Oxford, 1996, vol. 3, ch.17, pp 503-514.
4. A. Harada and M. Kamachi, *Macromolecules*, 1990, **23**, 2821-2823.
5. S. Loethen, J. M. Kim and D. H. Thompson, *Polym. Rev.*, 2007, **47**, 383-418.
6. C. L. He, S. W. Kim and D. S. Lee, *J. Control. Release.*, 2008, **127**, 189-207.
7. G. E. Newby, I. W. Hamley, S. M. King, C. M. Martin and N. J. Terrill, *J. Colloid. Interf. Sci.*, 2009, **329**, 54-61.
8. K. Patel, P. Bahadur, C. Guo, J. H. Ma, H. Z. Liu and K. Nakashima, *J. Disper. Sci. Technol.*, 2008, **29**, 748-755.
9. K. Patel, P. Bahadur, C. Guo, J. H. Ma, H. Z. Liu, Y. Yamashita, A. Khanal and K. Nakashima, *European Polymer Journal*, 2007, **43**, 1699-1708.
10. R. Ganguly, V. K. Aswal and P. A. Hassan, *J. Colloid. Interface. Sci.*, 2007, **315**, 693-700.
11. R. Ganguly, M. Kumbhakar and V. K. Aswal, *J. Phys. Chem. B*, 2009, **113**, 9441-9446.
12. Y. Kadam, R. Ganguly, M. Kumbhakar, V. K. Aswal, P. A. Hassan and P. Bahadur, *J. Phys. Chem. B*, 2009, **113**, 16296-16302.
13. L. Fan, M. Degen, N. Grupido, S. Bendle and P. Pennartz, *Mat. Sci. Eng. A-Struct.*, 2010, **528**, 127-136.
14. P. Parekh, R. Ganguly, V. K. Aswal and P. Bahadur, *Soft Matter*, 2012, **8**, 5864.
15. J. Joseph, C. A. Dreiss, T. Cosgrove and J. S. Pedersen, *Langmuir*, 2007, **23**, 460-466.
16. C. A. Dreiss, E. Nwabunwanne, R. Liu and N. J. Brooks, *Soft Matter*, 2009, **5**, 1888-1896.

17. M. Valero and C. A. Dreiss, *Langmuir*, 2010, **26**, 10561-10571.

18. C. Perry, P. Hebraud, V. Gernigon, C. Brochon, A. Lapp, P. Lindner and G. Schlatter, *Soft Matter*, 2011, **7**, 3502-3512.

19. J. Qin, X. W. Meng, B. J. Li, W. Ha, X. Q. Yu and S. Zhang, *J. Colloid. Interf. Sci.*, 2010, **350**, 447-452.

20. J. Huang, Z. Zhou, M. Wei, Y. Chen and P. R. Chang, *J. Appl. Polym. Sci.*, 2008, **107**, 409-417.

21. M. Valero and C. A. Dreiss, *Langmuir*, 2010, **26**, 10561-10571.

22. J. Szejtli, in *Comprehensive supramolecular chemistry*, ed. J. M. Lehn, Pergamon Press, Oxford, 1996, vol. 3, pp. 5-40.

23. M. Taghvaei and G. H. Stewart, *Anal. Chem.*, 1991, **63**, 1902-1904.

24. W. Y. Kuo and H. M. Lai, *Polymer*, 2011, **52**, 3389-3395.

25. I. V. Terekhova, O. V. Kulikov, R. S. Kumeev, M. Y. Nikiforov and G. A. Al'per, *Russ. J. Coord. Chem.*, 2005, **31**, 218-220.

26. S. X. Ji and J. Y. Walz, *J. Phys. Chem. B*, 2013, **117**, 16602-16609.

27. Y. C. Liang, G. Gillies, H. Patel, L. Matia-Merino, A. Q. Ye and M. Golding, *Food Hydrocolloid*, 2014, **36**, 245-255.

28. A. Guinier, *Ann. Phys. (Paris)*, 1939, **12**, 161-237.

29. M. A. J. Gillissen, M. M. E. Koenigs, J. J. H. Spiering, J. A. J. M. Vekemans, A. R. A. Palmans, I. K. Voets and E. W. Meijer, *J. Am. Chem. Soc.*, 2014, **136**, 336-343.

30. D. I. Svergun, *J. Appl. Crystallogr.*, 1992, **25**, 495-503.

31. S. W. Yeh, K. H. Wei, Y. S. Sun, U. S. Jeng and K. S. Liang, *Macromolecules*, 2005, **38**, 6559-6565.

32. S. R. Kline, *J. Appl. Crystallogr.*, 2006, **39**, 895-900.

33. L. K. Shrestha, O. Glatter and K. Aramaki, *J. Phys. Chem. B*, 2009, **113**, 6290-6298.

34. J. M. Franklin, L. N. Surampudi, H. S. Ashbaugh and D. C. Pozzo, *Langmuir*, 2012, **28**, 12593-12600.

35. S. Manet, A. Lecchi, M. Imperor-Clerc, V. Zholobenko, D. Durand, C. L. P. Oliveira, J. S. Pedersen, I. Grillo, F. Meneau and C. Rochas, *J. Phys. Chem. B*, 2011, **115**, 11318-11329.

36. H. C. Liao, C. S. Tsao, T. H. Lin, C. M. Chuang, C. Y. Chen, U. S. Jeng, C. H. Su, Y. F. Chen and W. F. Su, *J. Am. Chem. Soc.*, 2011, **133**, 13064-13073.

37. P. Debye, H. R. Anderson and H. Brumberger, *J. Appl. Phys.*, 1957, **28**, 679-683.

38. C. Travelet, P. Hebraud, C. Perry, C. Brochon, G. Hadziioannou, A. Lapp and G. Schlatter, *Macromolecules*, 2010, **43**, 1915-1921.

39. J. Dey, S. Kumar, S. Nath, R. Ganguly, V. K. Aswal and K. Ismail, *J. Colloid. Interf. Sci.*, 2014, **415**, 95-102.

40. S. Manet, A. Lecchi, M. Imperor-Clerc, V. Zholobenko, D. Durand, C. L. Oliveira, J. S. Pedersen, I. Grillo, F. Meneau and C. Rochas, *J. Phys. Chem. B*, 2011, **115**, 11318-11329.

41. T. E. Girardeau, T. J. Zhao, J. Leisen, H. W. Beckham and D. G. Bucknall, *Macromolecules*, 2005, **38**, 2261-2270.

42. A. Becheri, P. Lo Nostro, B. W. Ninham and P. Baglioni, *J. Phys. Chem. B*, 2003, **107**, 3979-3987.

43. A. Harada, *Coordin. Chem. Rev.*, 1996, **148**, 115-133.

44. P. Lo Nostro, J. R. Lopes, B. W. Ninham and P. Baglioni, *J. Phys. Chem. B*, 2002, **106**, 2166-2174.

45. H. Fujita, T. Ooya and N. Yui, *Macromol. Chem. Phys.*, 1999, **200**, 706-713.

46. M. Valero, C. Carrillo and L. J. Rodriguez, *Int. J. Pharm.*, 2003, **265**, 141-149.

536 Table. 1 Fit parameters for the DAB and cylindrical object model applied to SAXS
537 data for 5% PL F108 with 0, 1 and 9% β-CD addition.

Sample	length, L (nm)	Radius, R (nm)	β-CD per stack, N (number)	Characteristic length, ξ (nm)
5-0	8.20	1.02	---	28.3
5-1	1.23	0.62	1-2	18.3
5-9	2.37	0.64	3-4	15.5

538
539
540
541

Figure captions

Figure 1. Overview of the SAXS patterns of the eight samples studied. For clarity of presentation, the zero point of the intensity scale has been shifted to fit individual pattern.

Figure 2. Cross-sectional PDDFs for samples 5-0, 5-1 and 5-9.

Figure 3. Observed (open squares) and calculated (solid line) SAXS patterns of the sample 5-0. The dotted and dashed lines indicate, respectively, the contributions from the large-scale network appeared in the solution employing the DAB model and from the non-interacting cylinders of 1 nm in radius and 8 nm in length.

Figure 4. Observed (open squares) and calculated (solid line) SAXS patterns of the sample 5-19. The scattering profile can be decomposed into two components: the form factor P(q) (dashed line) and the structure factor S(q) (dotted line). The form factor P(q) contains the contributions from the lamellas (open circles) and cylinders (open triangles) in the sample.

Figure 5. Observed SAXS patterns of the dilute samples 5-0 (open squares), 5-1 (open circles), and 5-9 (open triangles). The solid line on each set of data indicates the calculated scattering profile of the corresponding sample. The schematic representation of the local (high q) and global (low q) structures of the samples 5-0 and 5-9 were shown as well.

Figure 6. Observed SAXS patterns of the dense samples 5-10 (open squares), 5-12 (open circles), 5-14 (open triangles), 5-16 (open diamonds), and 5-19 (open stars). The solid line on each set of data indicates the calculated scattering profile of the corresponding sample.

Figure 7. Observed (open circles) and calculated (solid and dashed lines) structure factors of the sample 5-10. The structure factor may be distinguished into tow separated sets of reflection, marked α-phase (solid line) of periodicity 50 nm and β-phase (dashed line) of periodicity of 96 nm. Only the first order reflection is revealed in each phase. The intensity of the α-phase is largely higher than that of the β-phase, showing the β–CD are mostly localized into the α-phase. The insets show the size distributions of the α-phase (left panel) and β-phase (right panel) obtained from the profile analysis.

Figure 8. Observed (open circles) and calculated (solid and dashed lines) structure factors of the sample 5-14. Reflections of up to the third order are revealed in both phases, with the periodicities of the α-phase and β-phases shrink to 32 and 41 nm, respectively. The insets show the size distributions of the α-phase (left panel) and β-phase (right panel) obtained from the profile analysis.

Figure 9. Observed (open circles) and calculated (solid and dashed lines) structure factors of the sample 5-19. Reflection peaks of up to the eighth order are revealed in the α-phase, while only the first order peak of the β-phase is

591 revealed. The insets show the size distributions of the α-phase (left panel)
592 and β-phase (right panel) obtained from the profile analysis.
593
594

595 Figure 1

596

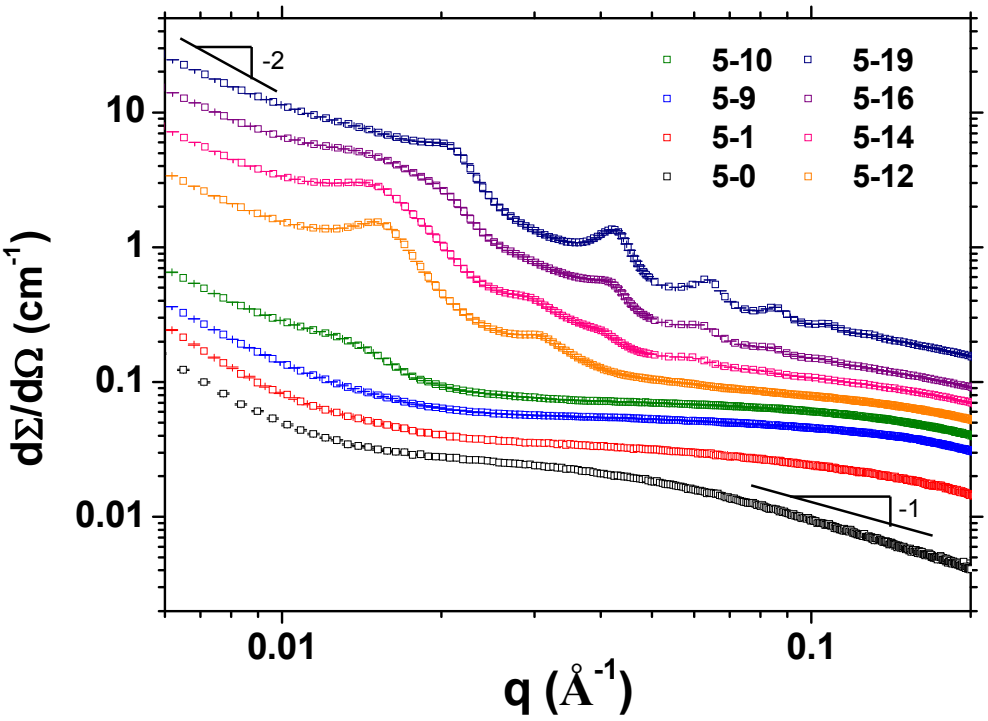

597 Figure 2

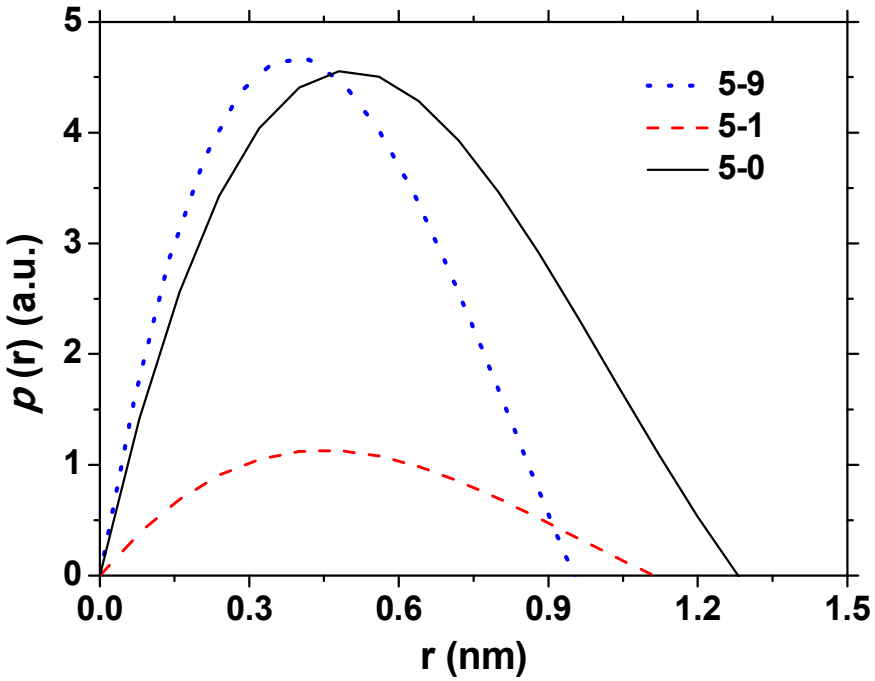

598

599

600 Figure 3

601

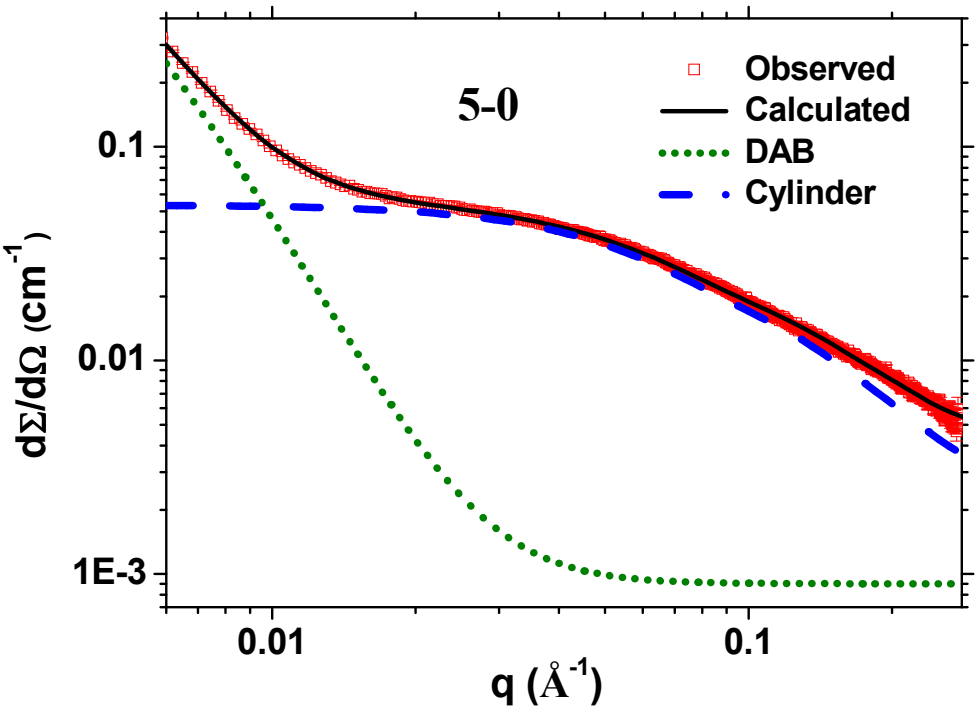

602 Figure 4

603

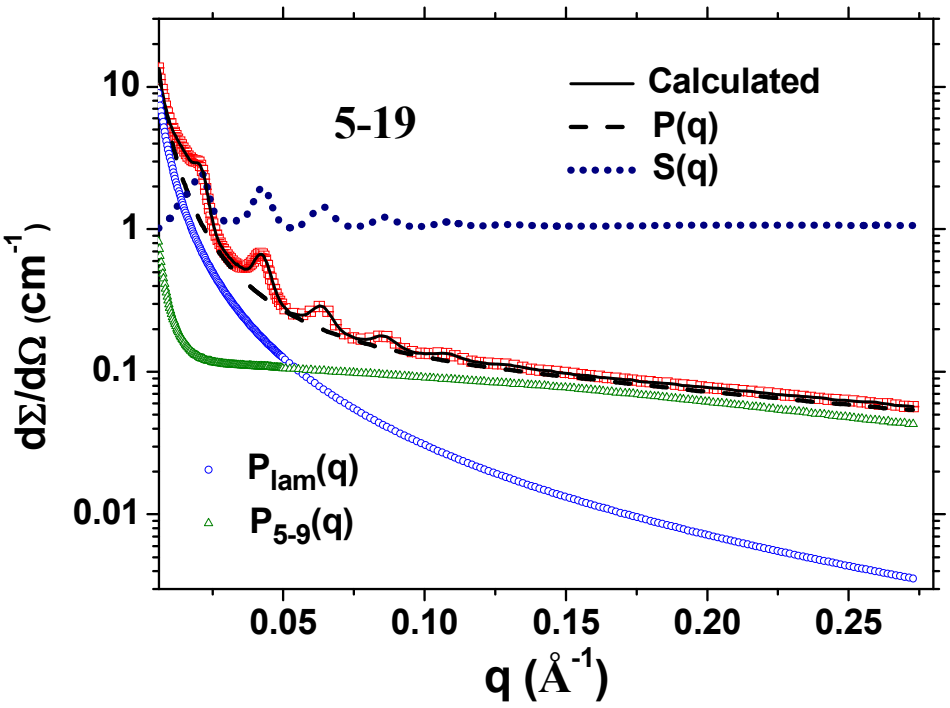

604 Figure 5
605

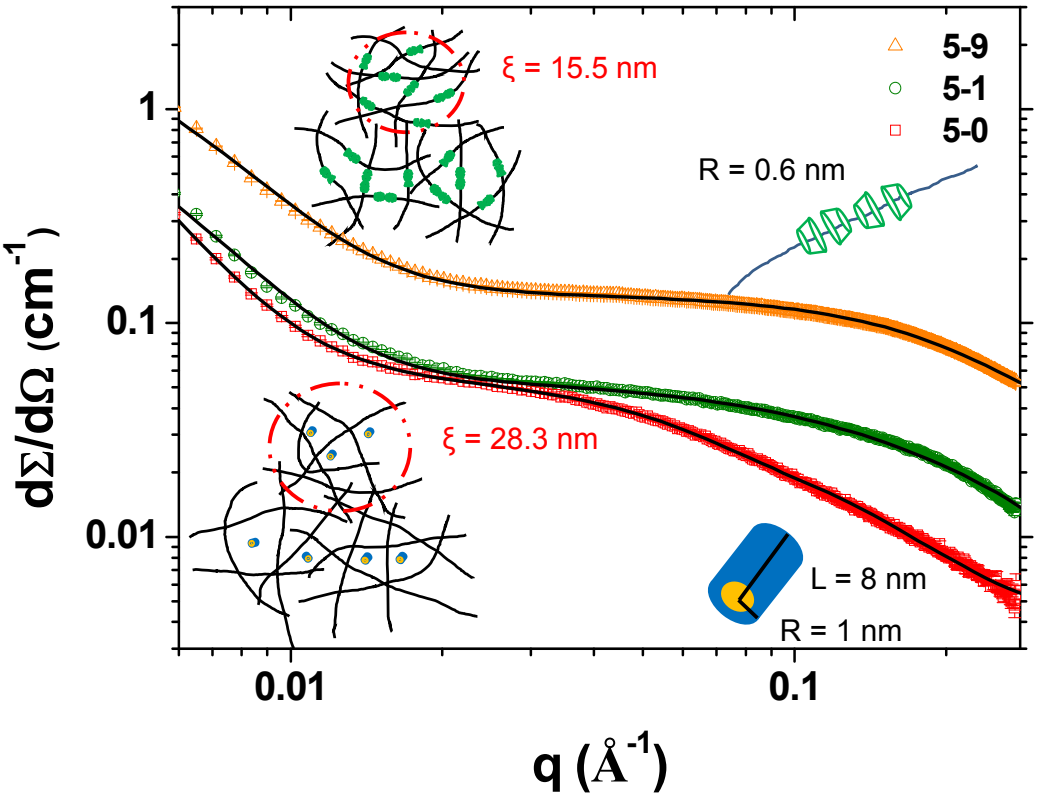

606 Figure 6

607

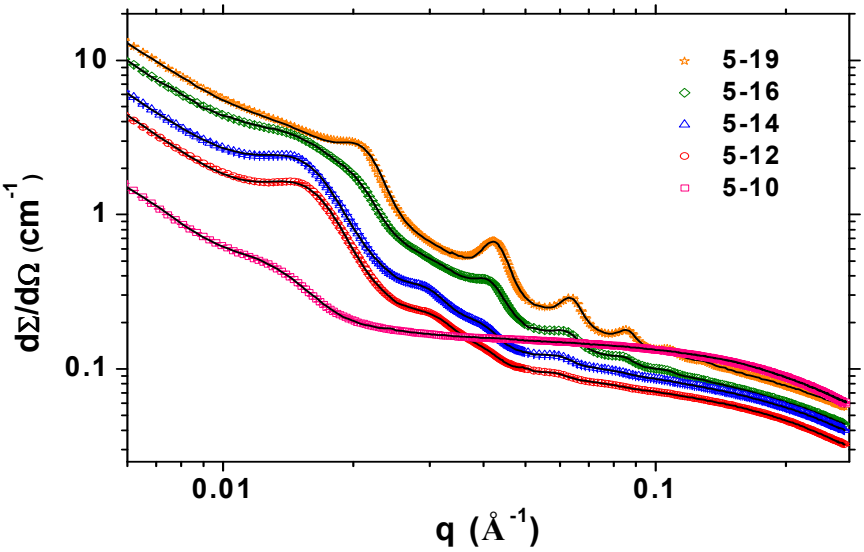

608 Figure 7

609

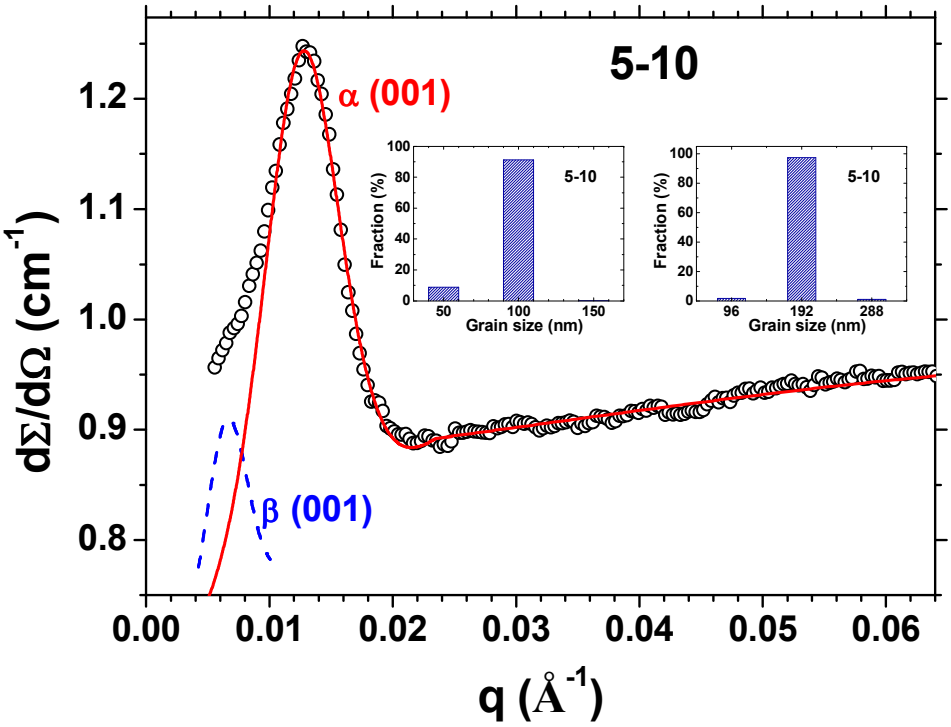

610 Figure 8

611

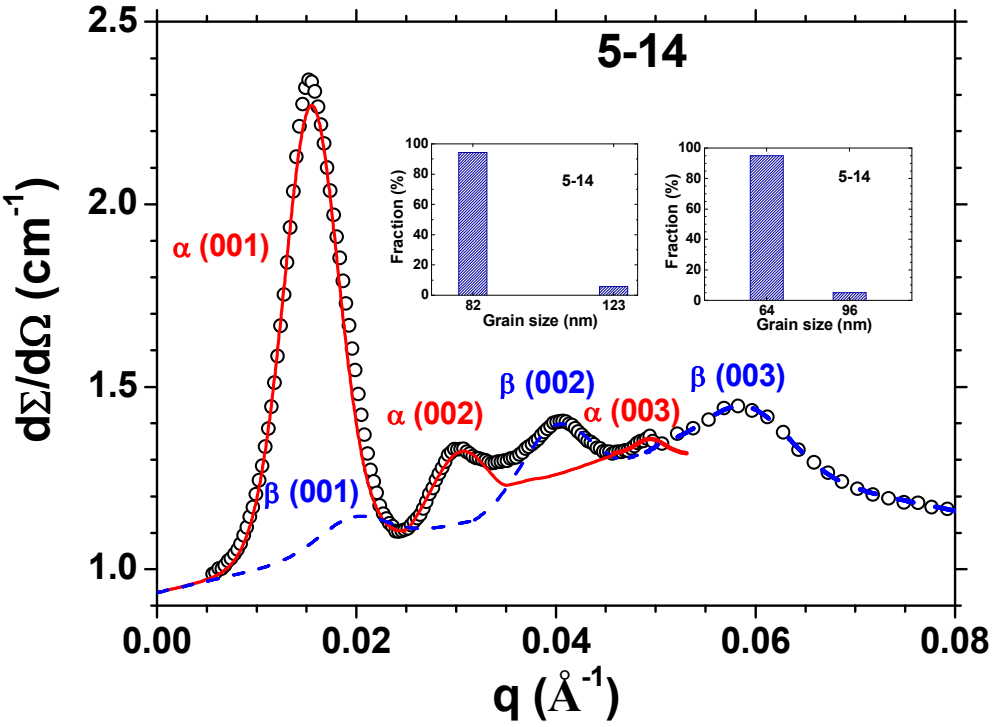

612 Figure 9

613

614

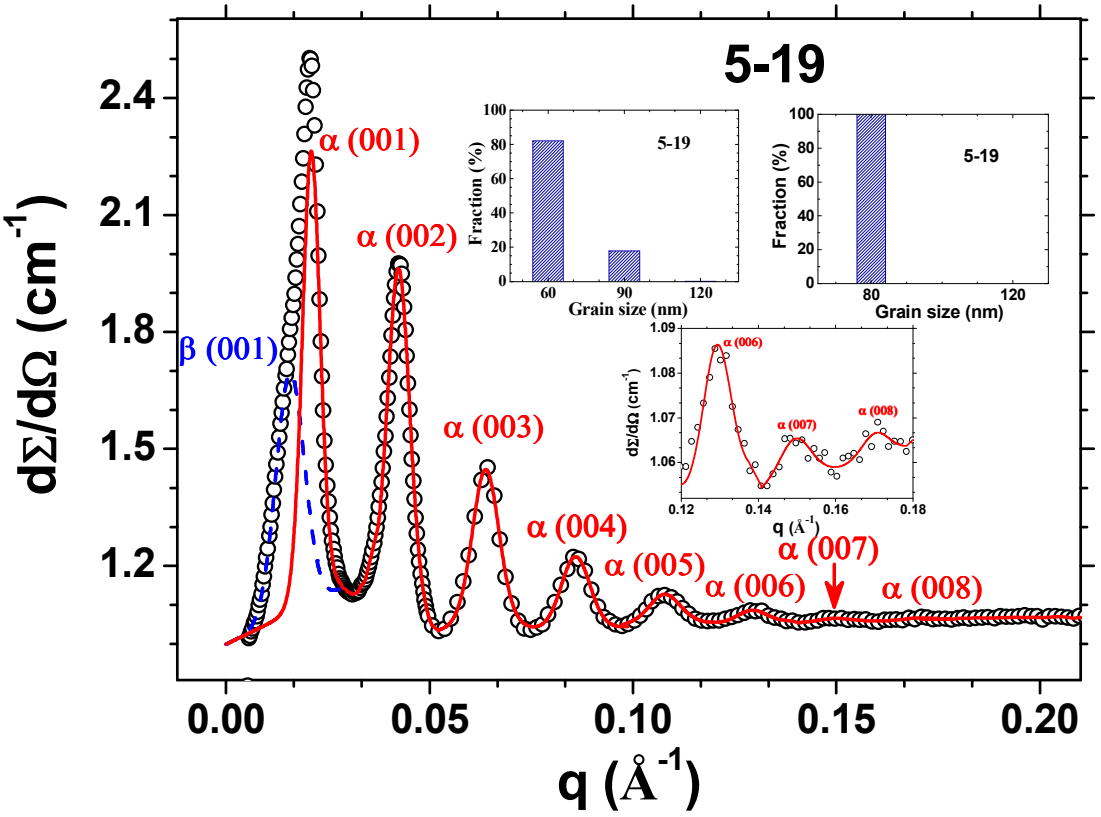

615 **Scheme captions**

616 Scheme 1. Schematic plots of the correlated structures of β-CD in samples (a) 5-10, (b)
617 5-12 and 5-14, and (c) 5-16 and 5-19.

618 Scheme 2. Schematic plots of the structures of PL F108 and correlated β-CD in
619 samples (a) 5-0, (b) 5-1, (c) 5-9, and (d) 5-19.

620

Scheme 1

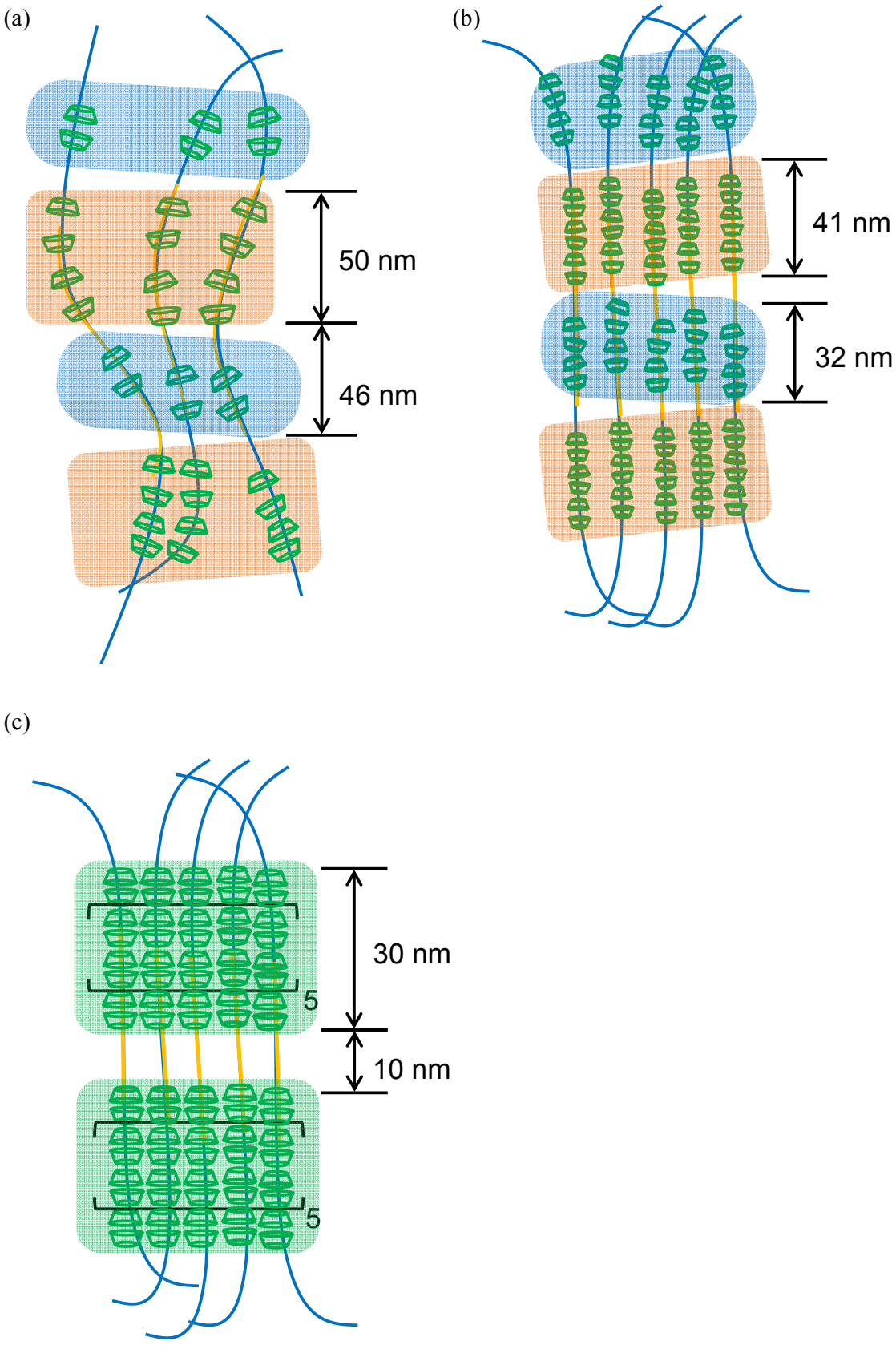

635 **Scheme 2**

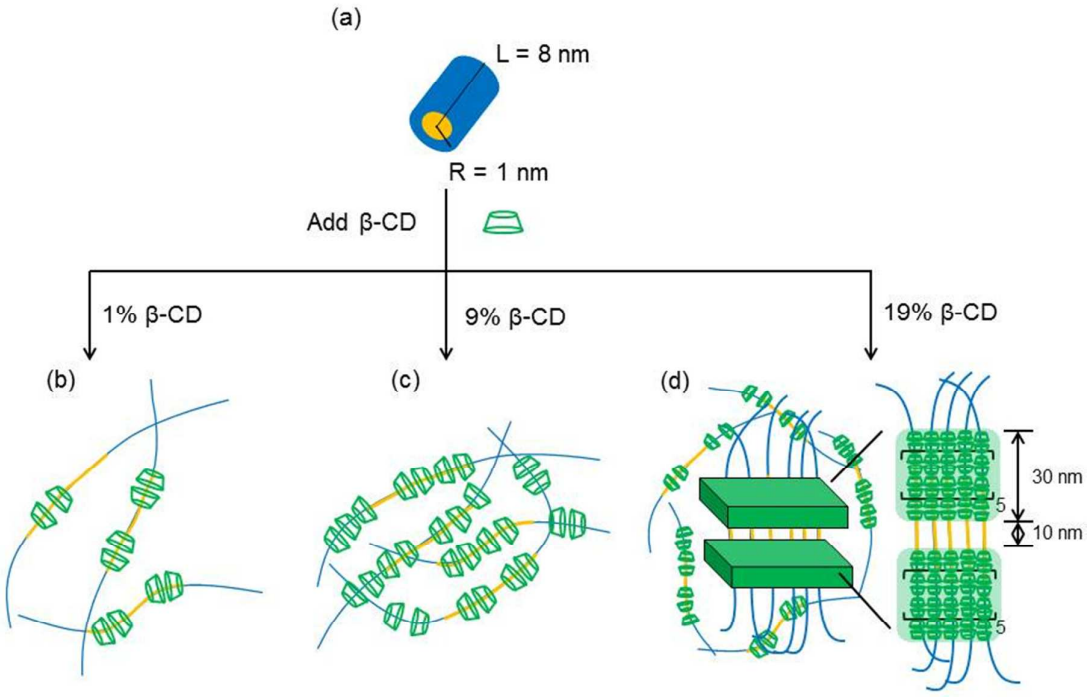

636

Graphical Abstract